Journal of Materials Chemistry A

Strong, Thermo-Reversible Salogels with Boronate Ester Bonds as Thermal Energy Storage Materials

Journal:	*Journal of Materials Chemistry A*
Manuscript ID	TA-ART-08-2022-006183.R2
Article Type:	Paper
Date Submitted by the Author:	22-Sep-2022
Complete List of Authors:	Rajagopalan, Kartik Kumar; Texas A&M University, Materials Science and Engineering Zhu, Xiuzhu; Texas A&M University, Materials Science and Engineering Sukhishvili, Svetlana; Texas A&M University, Department of Materials Science and Engineering;

Strong, Thermo-Reversible Salogels with Boronate Ester Bonds as Thermal Energy Storage Materials

Kartik Kumar Rajagopalan[#], Xiuzhu Zhu[#], and Svetlana A. Sukhishvili[*]

Texas A&M University, Department of Materials Science & Engineering,

College Station, TX 77843, USA

[#] Authors contributed equally to this work

Abstract

Inorganic salt hydrates are promising phase change materials (PCMs) but suffer from low viscosity at temperatures above their melting point resulting in leakage problems during thermal storage applications. To achieve shape stabilization of one type of molten inorganic PCM – calcium nitrate tetrahydrate (CNH) – this work explored gelation of polyvinyl alcohol (PVA) in this solvent and the effect of dynamic boronate ester bonds on salogel strength. The occurrence of gelation of PVA in molten CNH but not in water is rationalized by the extremely high salt content and scarcity of hydration water in CNH, enabling intermolecular hydrogen bonding between PVA chains. While neat PVA salogels in CNH were weak, with a gel-to-sol transition temperature (T_{gel}) below room temperature, the addition of small amounts of borax (<~0.3 wt%) introduced dynamic covalent crosslinks and yielded salogels with T_{gel} tunable over a wide temperature range from 7 to 70 °C. The PVA-borax salogels were about one order of magnitude stronger than their well-known PVA/borax hydrogel counterparts, and, unlike PVA/borax hydrogels, were capable of retaining their shape and preventing leakage of molten CNH. Moreover, the salogels exhibited reversible and repeatable temperature-triggered gel-to-sol transitions and the ability to self-heal. The low polymer and crosslinker concentration also ensured that more than 95% of the heat of fusion of neat CNH was maintained in the salogels and was retained after twenty cycles of melting and crystallization, demonstrating the robust nature of these energy storage materials.

Introduction

Thermal energy is the most consumed form of energy that is available in many forms such as fossil fuels, solar thermal energy, geothermal energy, biomass, and as industrial waste heat. For optimal utilization and preservation of these sources, several thermal energy storage strategies and thermal storage materials are being explored.[1] One example is phase change materials (PCMs), whose capability of storing and releasing large amounts of thermal energy as latent heat during phase transitions can be used for thermal management in buildings to reduce energy consumption through either direct incorporation in the building walls or use in heat and cold storage units.[1,2] Among several types of PCMs that include organic and inorganic materials, inorganic salt hydrates composed of inorganic salt and water stand out as low-cost, non-flammable materials with high heat storage capacities.[3] However, low viscosity of molten inorganic salt hydrates leads to leakage from the thermal storage module.[2, 3] Several strategies using inorganic matrices and polymer networks were developed to provide shape stabilization of the salt hydrate in its liquid state.[3-8] Polymers such as polyacrylamide,[4, 8] self-curing acrylic resin,[5] UV cured polyurethane acrylate,[6] and poly(acrylate sodium)[7] have been used as shape stabilizing matrices for salt hydrates and their eutectics. PCM loading varying from 42 to 90 wt% were reported with these matrices, which resulted in a lowering of heat of fusion and changes in the phase change temperature of the salt hydrate PCM.[4-8] However, these efforts were focused on developing materials that are permanently crosslinked,[4-8] which makes the removal of the PCM from heat exchange modules difficult at the end of their life cycle. In contrast, temperature-responsive property of the shape stabilizing matrix allows for easy filling and removal of the PCM from thermal storage module due to their ability to reversibly transition from gel to sol above a gel transition temperature (T_{gel}).

Our previous work introduced temperature-responsive polymer gels (salogels) in molten inorganic salt hydrates using hydrogen bonding polymers and physical crosslinkers.[9, 10] We established that molten salt hydrates present a unique class of solvents for hydrogen-bonding polymers, such as poly(vinyl alcohol) (PVA), resulting in gelation which does not occur in water.[11] The reason for such a behavior was identified as scarcity of water in these high-ionic-content solvents (~55 wt% of salt in case of lithium nitrate tetrahydrate, LNH). Our recent publication compared the inorganic salt hydrates ($AB{\cdot}nH_2O$, A and B are cations and anions) with water, aqueous salt solutions, and ionic liquids as polymer solvents and discussed the effects of solvent structure and polymer-solvent interactions on polymer solvation and gelation.[3] The unique

behavior of polymers in these solvents is due to incomplete saturation of the hydration shells of ions and poor hydration of polymer chains by n moles of water.[3] This deficiency sets a strong competition between ions and polymers for water molecules, making molten salt hydrates a unique media for dissolution or gelation of organic compounds and polymers.[3, 11, 12] Our work also revealed that the use of the physical crosslinking strategy for salogel strengthening requires addition of significant amount of a crosslinker which is unfavorable for maintaining the heat of fusion characteristics of the neat PCM, and also leads to crosslinker clustering [10, 13]

This work explores a novel approach for shape stabilization of inorganic salt hydrate PCMs using polymer gels crosslinked by dynamic covalent boronate ester bonds. In contrast to physically crosslinked gels which lack mechanical strength and covalently crosslinked gels which are irreversible, dynamic covalent bonds confer the strength of a covalent bond resulting in a strong gel network necessary for shape stabilization, while the dynamic nature of the bonds result in reversible deconstruction of the gel network in response to an external stimuli. Boronate ester bonds are well known to modulate strength and impart pH- and temperature responsiveness to solvent-free polymer networks[14] and hydrogels,[14-30] but their action in the environment of inorganic PCMs remained unexplored. A PCM of choice for this work was calcium nitrate tetrahydrate ($Ca(NO_3)_2 \cdot 4H_2O$, CNH), an inexpensive material with a heat of fusion of 153 kJ/kg and low viscosity of 67 mPa s at 323 K above its melting temperature of 42 °C which increases its propensity for leakage.[31, 32] The high ion content (e.g. ~69 wt% calcium nitrate in CNH) and scarcity of water in inorganic PCMs result in incomplete hydration of ions and polymer chains[3, 33] favoring intermolecular polymer-polymer hydrogen bonding and formation of weak PVA salogels. Addition of borax in small amounts dramatically strengthened the PVA salogels and increased its T_{gel} well above the melting point of CNH, while maintaining temperature-responsiveness allowing for on-demand deconstruction at the material's end-of-life. In contrast to the well-known boronate ester hydrogels, the salogels were stronger and also demonstrated shape retention capability. The dynamic covalent boronate ester salogels with a high PCM loading (>96 wt%) showed excellent shape stabilization capability, leakage prevention, and retention of thermal properties over multiple melting-crystallization cycles. The PVA/borax salogels reported here demonstrate a novel application of the well-known boronate ester bonds as thermal energy storage materials. The salogels had a very high PCM content (>96 wt%), which is significantly higher than that reported with other polymer matrices,[4-8] allowing retention of most of the heat fusion capacity of the

material. Moreover, the salogels could be deconstructed on demand at the material's end-of-life due to repeatable thermo-reversibility of gelation.

Materials and Methods

Materials

$PVA_{90k,98}$ (molecular weight 90 kg /mol, hydrolysis percent 98%), $PVA_{60k,98}$ (molecular weight 60 kg/mol, hydrolysis percent 98%), $PVA_{90k,87}$ (molecular weight 90 kg/mol, hydrolysis percent 87%), $PVA_{20k,98}$ (molecular weight 20 kg/mol, hydrolysis percent 98%), and sodium tetraborate decahydrate (ACS, 99.5-105.0%) were purchased from Alfa Aesar and used as received (**Table 1)**. Calcium nitrate tetrahydrate (ACS, 99.0-103.0%) was purchased from Alfa Aesar and purified by passing through a PTFE (0.45 μm, 40 mm) syringe filter. Deuterium oxide (D_2O) with 99.9 atom % was purchased from Sigma-Aldrich and used as received. Ammonium hydroxide (28-30%) were purchased from VWR International and used as received.

Table 1. Abbreviations for different PVA used to make salogels

Abbreviation	Molecular weight	Hydrolysis degree
$PVA_{90k,98}$	90 kg/mol	98%
$PVA_{60k,98}$	60 kg/mol	98%
$PVA_{90k,87}$	90 kg/mol	87%
$PVA_{20k,98}$	20 kg/mol	98%

Preparation of salogels and hydrogels

Liquid CNH was obtained by heating as-received solid CNH up to 50 °C in a sealed vial. PVA/CNH salogels were prepared by adding PVA powders into liquid CNH and heating the mixtures at 80 °C on a hot plate under gentle stirring for 24 hours in a sealed vial. The polymer readily dissolved in CNH upon heating to 80 °C with gentle stirring, whereas PVA dissolution in water required heating to above 95 °C with vigorous stirring regardless of molecular weight and degree of hydrolysis. After the PVA was completely dissolved, stirring was stopped, and the samples were put into the oven at 80 °C for 24 hours to remove bubbles and obtain a homogeneous solution. The samples were then cooled down to room temperature to induce gelation. PVA/borax salogels were prepared by adding borax to $PVA_{90k,98}$ salogel at 70 °C, followed by heating the mixture to 90 °C while stirring to facilitate the dissolution of borax, and cooling down to room

temperature to induce gelation. Due to the limited solubility of borax in CNH the maximum amount of the crosslinker that could be dissolved was ~0.35 wt%, therefore borax concentrations not exceeding 0.35 wt% were used in all salogels. For shape stabilization studies which required the strongest gels, borax concentration of 0.32 wt% was used. Because of the known supercooling effect that is significant in the case of CNH,[34] no crystallization occurred in the system at room temperature, and freezing temperatures (-18 °C) were used to induce crystallization of CNH for testing performance of the matrix during multiple crystallization/melting cycles.

PVA/borax hydrogels were prepared by dissolving $PVA_{90k,98}$ in water as described, cooling PVA aqueous solutions to room temperature, followed by the addition of borax and stirring at room temperature until the borax dissolved and formed a gel. Stirring was stopped at this point and the gel was allowed to equilibrate at room temperature for 24 hours for homogenization.

Deuteration of CNH for ATR-FTIR studies

The use of deuterium oxide (D_2O) instead of H_2O with salogels and hydrogels enabled distinguishing the -OH stretching band of water from the salt hydrate from the -OH stretching band of PVA. To prepare the deuterated analogue of CNH, i.e. CND, CNH was first heated in a vacuum oven at 135 °C to remove water and form anhydrous calcium nitrate. Then anhydrous calcium nitrate salt was mixed with the stoichiometric amount of D_2O to obtain CND. Analysis by attenuated total reflection Fourier transform infrared spectroscopy (ATR-FTIR) showed the disappearance of -OH peak (3000-3800 cm^{-1}) and the appearance of -OD peak (2100-2800 cm^{-1}) after the completion of the above procedure, thus confirming the successful deuteration of CNH (**Fig. S1**).

Materials Characterization

ATR-FTIR measurements were performed using a Bruker Tensor II spectrometer equipped with a mercury cadmium telluride (MCT) detector and a single-reflection diamond ATR attachment. Spectra was collected in the range of 400-4000 cm^{-1} at 4 cm^{-1} resolutions using 64 repetitious scans. Each measurement was performed with ~10 μL of sample drop-casted on to the ATR diamond crystal.

Peak fitting procedure and analysis of vibrational features of D_2O and CND. FTIR analysis of solvents, and PVA salogels and hydrogels shown in **Figs. 1** and **2** was performed using deuterated solvents (D_2O or CND). Peak fitting of the OD peak of D_2O was done based on Sun's 5 sub-bands theory which considers single donor double acceptor (DAA, strong, 2300 cm^{-1}),

double donor double acceptor (DDAA, strong, 2385 cm^{-1}), single donor single acceptor (DA, weak, 2479 cm^{-1}), double donor single acceptor (DDA, weak, 2574 cm^{-1}) hydrogen bonding modes, and free OD (2668 cm^{-1}) **(Fig. 1a).**[35] The fitting results were obtained by assuming the 5-

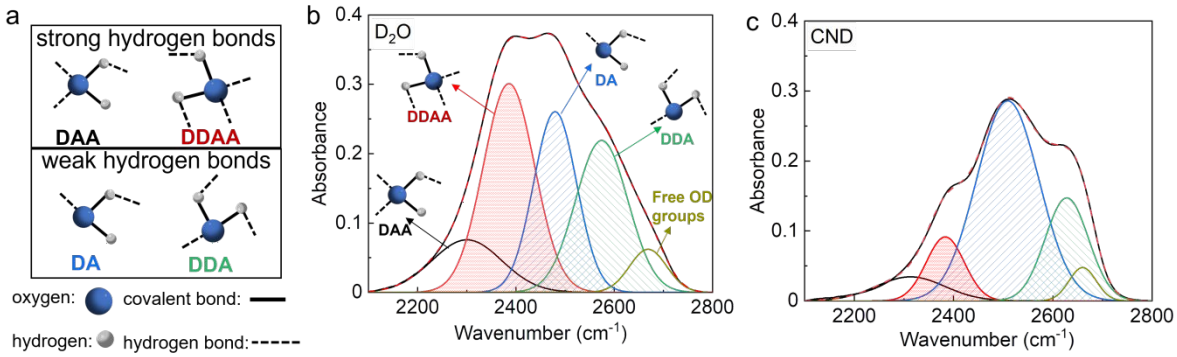

Fig. 1. ATR-FTIR analysis of 2100-2800 cm^{-1} OD stretching vibrational band in CND and D_2O. (a) Schematic of DAA, DDAA, DA, and DDA hydrogen bonding modes; (b) D_2O and (c) CND spectra fitting of OD band.

sub peaks are Gaussian. For D_2O, the peak centers and bandwidths were taken from published data.[36] These fitting parameters were used to obtain a suitable initial fitting for both D_2O and CND and then the parameters were allowed to vary at the final step of fitting. Before curve fitting, a baseline correction was performed to the raw spectra. **Fig. 1b & c** show that the OD stretching vibrational features dramatically differ in D_2O and liquid CND, indicating the different state of water in these two solvents. The most notable trend is the dominance of larger DDAA ($(H_2O)_{16}$, $(H_2O)_{20}$)[37, 38] and smaller DA ($(H_2O)_6$)[37, 38] clusters in water and CND, respectively.

Rheological Measurements. Rheological measurements for both salogel and hydrogel samples were performed using an Anton-Paar stress-controlled rheometer (MCR 301) equipped with a Peltier stage that enabled controlling the temperature within ±0.5 °C. All measurements were performed using parallel plate with a 40 mm diameter and a gap of 800 µm. The linear viscoelastic regime (γ_L) was determined by oscillation amplitude sweep tests which were conducted at 25 °C within a strain range of 0.1−100% using a frequency of 10 rad/s. The oscillation temperature ramp and oscillation frequency sweep experiments were performed in the linear viscoelastic regime at a frequency of 10 rad/s and 6% strain. To illustrate the self-healing property, oscillation time sweeps were alternatively conducted in the linear and non-linear viscoelastic

regimes to simulate rupture and recovery of the gels. Water evaporation and absorption during the experiment was minimized using a solvent trap.

Thermal Analysis. The melting temperatures and heat of fusion of salogels were determined by differential scanning calorimetry (DSC) using a TA Instruments Q2000 calorimeter with a temperature precision of ±0.005 °C and calorimetric precision of ±0.25%. Measurements were conducted at a 10 °C/min temperature ramp from -40 °C to 80 °C under nitrogen gas purging at a flow rate of 50 mL/min.

Thermal cycling of salogels

The ability of PVA/borax salogels to shape stabilize CNH and preserve its thermal properties during thermal cycling was evaluated by subjecting salogels to multiple melting and crystallization cycles. Salogels containing 3 wt% $PVA_{90k,98}$ and 0.32 wt% borax were chosen for these experiments since this system provided the strongest gel required for shape stabilization studies. Shape stabilization experiments were performed using hexagon shaped salogels obtained by crystallizing the as prepared salogels in molds. Thermal cycling was done by heating the bulk salogels stored in an air-tight container to 50 °C, *i.e.* a temperature above the melting point of CNH (42 °C) and holding at this temperature until all the CNH melted. Because CNH does not crystallize when cooled below its melting point due to supercooling, crystallization was achieved by putting the salogels in the freezer at -18 °C until crystallization occurred, which took at least 12 hours to complete.[39]

A similar procedure as described above was used to study the ability of the salogels to preserve the thermal properties of CNH during thermal cycling. However, in this case the melting and crystallization cycles were performed ex-situ with ~10 grams of salogel contained in a sealed round bottom flask. The ex-situ experimental design was needed due to the high degree of supercooling, which did not result in crystallization of CNH during the cooling step in DSC even at a low cooling rate of 1 °C/min. Melting was achieved by heating the flask to 50 °C and crystallization was achieved by exposing the flask containing the salogel to liquid nitrogen. Complete crystallization required exposure to liquid nitrogen until crystallization was initiated followed by storage in a freezer at -18 °C for at least 12 hours. Small samples (5-10 mg) of crystallized salogel were taken for DSC measurements to determine thermal properties at desired intervals up to twenty cycles.

Results and discussion

The propensity of PVA – a polymer that is prone to both polymer-polymer and polymer-water hydrogen bonding – is strongly dependent on the type of solvent and the state of solvation of polymer chains. **Fig. 1** shown in the Materials and Methods section highlights the dramatic differences in hydrogen bonding of water molecules in aqueous and salt hydrate solvents, with large water clusters characteristic of strong hydrogen bonding in bulk water broken into smaller clusters in the salt hydrate. The scarcity of water in the system leaves hydration shells of Ca^{2+} and NO_3^- ions in CNH only ~33% saturated[3] that can impact hydration state of dissolved polymers. **Fig. 2** shows the ATR-FTIR data in the -OH stretching region of $PVA_{20k,98}$ chains dissolved in aqueous and salt hydrate solvents. The use of the deuterated rather than hydrogenated solvents allowed us to selectively observe -OH stretching vibrations of PVA and correlate the observed wavenumbers with the degree of hydrogen bonding of PVA with surrounding solvent. It is seen that the band for stretching vibrations of -OH groups in PVA is significantly blue shifted from 3396 cm^{-1} in heavy water to 3447 cm^{-1} in CND, suggesting dehydration of PVA chains in the molten salt hydrate. Schematic in **Fig. 2** illustrates the resultant enhancement of PVA-PVA hydrogen bonding and PVA-ion interactions in the salt hydrate solvents, and the suppression of these interactions in aqueous environment by the abundant hydration of PVA. Consequently, as shown in **Fig. 2**, when $PVA_{90k,98}$ solutions were first heated to 80 °C to dissolve PVA and then cooled to room temperature, gelation occurred in CNH but not in H_2O. Note that the reported PVA hydrogels in water required not only high PVA concentrations (>15 wt%) but also additional freeze/thaw processing to promote kinetic trapping of dehydrated PVA units within crystalline domains of the gel junction points.[40, 41] In contrast, $PVA_{90k,98}$ spontaneously gelled in CNH at moderate concentrations of 3-6 wt%, forming neat PVA salogels.

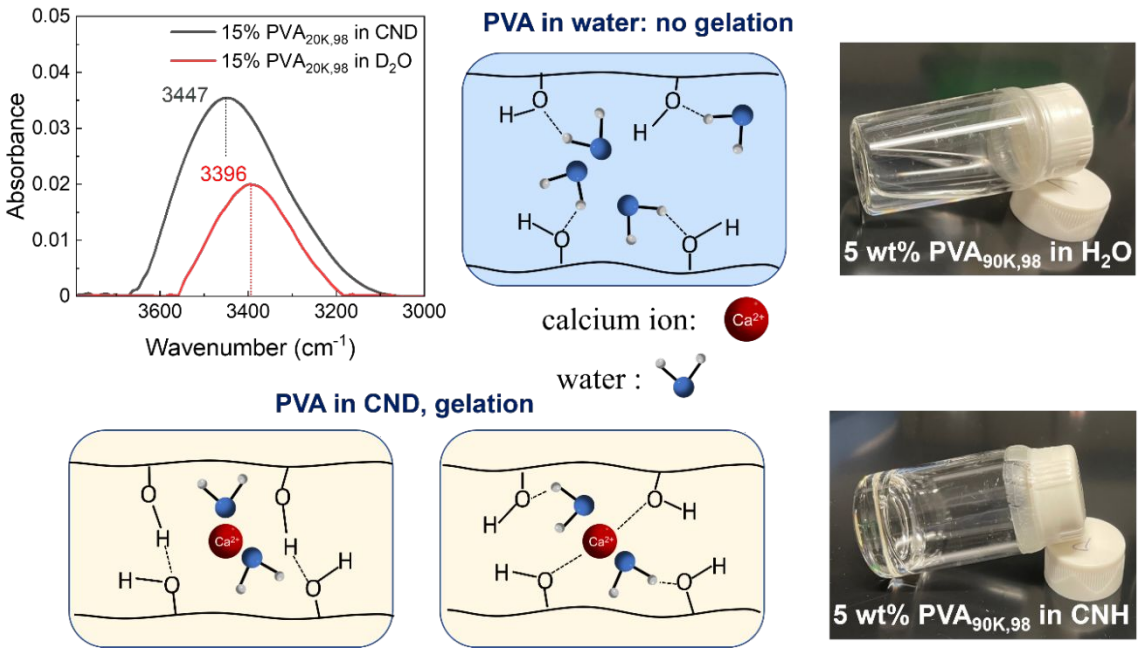

Fig. 2. ATR-FTIR spectra showing changes in -OH stretching region of $PVA_{20k,98}$ in deuterated water and CNH (D_2O and CND, respectively), schematic of suggested differences in PVA hydration and hydrogen-bonding in two solvents, as well as images of glass vials containing 5 wt% $PVA_{90k,98}$ in water and CNH. Experiments were performed at 25 ˚C.

Fig. 3a,b show that the crosslinker-free PVA salogels were relatively weak (with G' and G'' in the kPa range) but exhibited the gel-sol transition as a result of temperature-triggered weakening of interchain hydrogel bonding. The gelation temperature, T_{gel}, determined from oscillatory temperature sweep experiments as the crossover point of storage modulus (*G'*) and loss modulus (*G"*)[9, 42] at a frequency of 10 rad/s after the strain sweep experiments to determine the linear viscoelastic regime (**Fig. S2**). The T_{gel} was frequency dependent and varied by 8 °C for PVA salogels when temperature sweeps were performed between 3 and 10 rad/s (data not shown), suggesting that the salogels did not follow the rheological definition of true gels which requires the phase angle δ (tan δ = *G"/G'*) to be independent of frequency.[43, 44] This behavior is further highlighted in **Fig. S3** showing that in high frequency regime beyond the modulus crossover both storage and loss moduli continued to increase. Note that the frequency-dependent behavior of the crossover point was broadly reported for many physical gels,[9, 45, 46] including borax-crosslinked systems,[47, 48] and often explained by heterogeneity and clustering of weak physical crosslinks,[13, 49]

which is likely to occur in the borax-free PVA salogels stabilized by intermolecular hydrogen bonding. **Fig. 3c, d** and **Fig. S3** illustrate the effects of molecular weight and degree of hydrolysis on T_{gel} strength and relaxation time of PVA salogels. Consistent with prior reports on the effect of molecular weight on polymer gelation which were demonstrated in other systems,[50, 51] PVA with matched concentration and degree of hydrolysis, but higher molecular weight had enhanced T_{gel} (**Fig. 3c**) and longer relaxation time τ (**Fig. S3a, b**), as demonstrated for $PVA_{90k,98}$ and $PVA_{60k,98}$. The effect of molecular weight is explained by higher number of elastically active chains resulting in large number of connected junction zones forming a percolating network.[50, 51] The gelation temperature and relaxation time (**Fig. 3d** and **S3c, d**) also increased with the degree of hydrolysis of PVA, indicating the important role of intermolecular hydrogen bonding between PVA hydroxyl groups in gelation.[52] PVA with higher degree of hydrolysis provided more -OH groups for forming physical crosslinking points, facilitating the formation of a 3D network.

For the use of CNH-based salogels in heat storage applications, preservation of melting point and high heat of fusion of salogels compared to that of neat CNH is critically important. **Fig. 3e** and **f** show the representative DSC curves and the melting points and heats of fusion obtained from DSC data analysis. Comparison of melting peaks of neat CNH and $PVA_{90k,98}$/CNH salogels shows that the difference in the melting points was as low as 1 °C (**Fig. 3e**), and reduction of heat of fusion of neat CNH was proportional to the amount of PVA added, with more than 95% of the heat of fusion compared to neat CNH retained in a 4 wt% $PVA_{90k,98}$ salogel (**Fig. 3f**). Note that similar results were obtained with PVA of different molecular weights (90 kDa and 60 kDa, **Fig. S4**). The data suggest that solid-liquid phase transition of CNH was not affected by the addition of the polymer and that the heat of fusion decreased mainly due to dilution of CNH by PVA, with the interactions between PVA and CNH playing a negligible role in thermal performance of PVA/CNH salogel system.

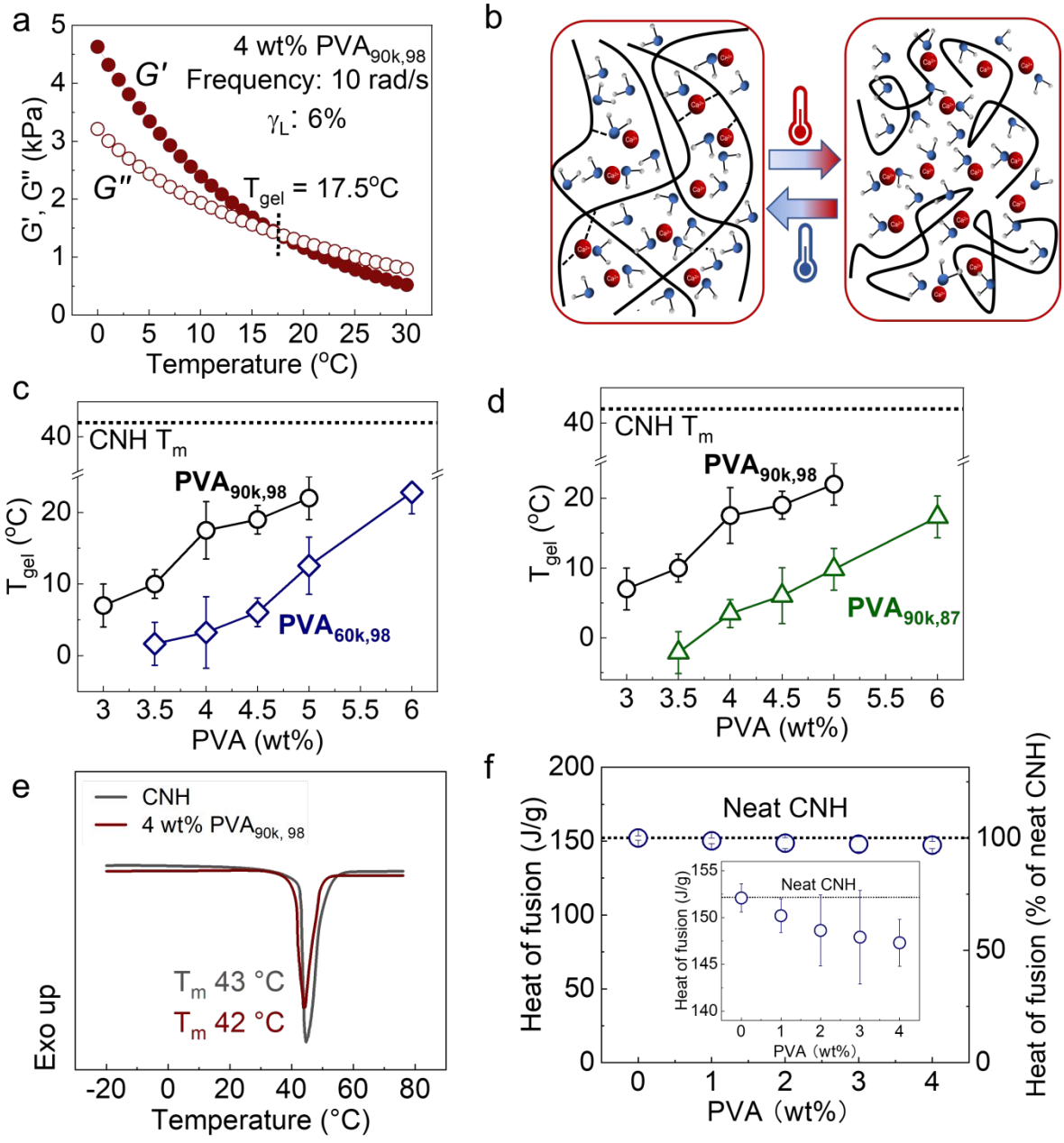

Fig 3. (a) Oscillatory rheology temperature sweep experiment performed at 10 rad/s showing gel to sol transition temperature (T_{gel}) in 4% $PVA_{90k,98}$ salogels (b) Schematics of the gel-to-sol transitions in PVA salogels. (c, d) Effects of molecular weight and degree of hydrolysis of PVA on T_{gel} in PVA salogels. (e) DSC curves comparing the melting peaks of neat CNH and 4 wt% $PVA_{90k,98}$ salogel. (f) The effect of PVA concentration on heat of fusion of CNH in $PVA_{90k,98}$ salogels.

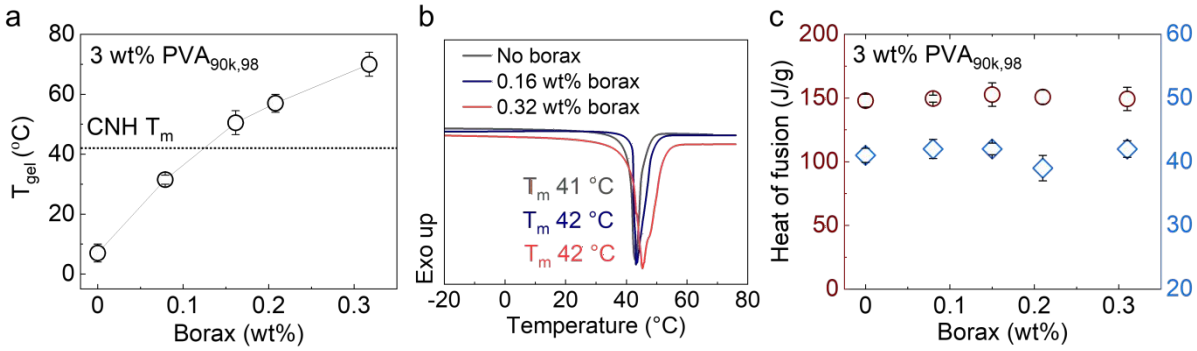

Fig. 4. (a) Effect of borax concentration on T_{gel} of salogels determined from temperature sweep rheology and (b) DSC curves showing the melting transition of CNH in salogel without borax and upon addition of 0.16 and 0.32 wt% borax. (c) Heat of fusion and melting point of CNH as a function of borax concentration for $PVA_{90K,98}$/borax salogels.

As shown in **Fig. 3**, crosslinker-free salogels were relatively weak and exhibited T_{gel} far below the melting point of CNH of 42 °C. To improve strength of the salogels and achieve T_{gel} above the melting point of CNH, we introduced dynamic covalent bonds via addition of borax. Formation of dynamic covalent borate-diol ester bonds has been shown to be exothermic, with equilibrium shifting toward the initial components with increasing temperature.[29, 53] We expected that introduction of these bonds in the salogel can improve the gelation strength while maintaining the salogel temperature responsiveness. **Fig. 4a** shows the effect of borax concentration on T_{gel} of $PVA_{90k,98}$ salogels. Importantly, the addition of as small amount as 0.16 wt% of borax dramatically improved T_{gel} by almost 40 °C, resulting in salogels with T_{gel} higher than the melting point of CNH (**Fig. S5**). At the same time, relaxation time of $PVA_{90k,98}$/borax salogels increased exponentially with borax concentration (**Fig. S6**). Specifically, addition of 0.32 wt% borax to 3 wt% $PVA_{90k,98}$/CNH system raised T_{gel} to 70 °C and caused 3 orders of magnitude increase in the relaxation time compared to a PVA salogel without borax. The thermo-responsive gelation in PVA/borax salogels remained reversible as demonstrated using a 0.16 wt% borax salogel with a T_{gel} of 46 °C by 3 heating/cooling cycles between room temperature and 70 °C (**Fig. S7**). Moreover, the addition of a small amount (<0.3 wt%) of borax to the salogels had a negligible effect on the CNH melting point and heat of fusion of the salogels (**Fig. 4b, c**). Hence, borax provides effective strengthening of the salogels, as well as supports their temperature-responsive behavior which can be tuned by the number of boronate ester bonds introduced. Crucially, for

thermal energy storage applications the phase transitions and thermal properties of the salt hydrate PCM are not impacted by the dynamic covalent boronate ester bonds.

The addition of borax also allowed controlling the salogel strength by tuning the pH of the system. To explore this effect, 3 wt% $PVA_{90k,98}$ salogels with 0.16% borax (T_{gel} = 46 °C) were used, in which the original pH (pH=6) was adjusted to higher values using ammonium hydroxide. **Fig. S8(a, b)** shows that as pH was increased to 7, *G'*(ω) exceeded *G"*(ω) in the entire frequency range 0.1-300 rad/s, indicating a dramatic increase in the relaxation time τ, likely due to the formation of additional boronate ester bonds enabled by pH-assisted conversion of boric acid to borate anions. Consistent with this result, raising pH from 6 to 7 for PVA/borax salogels led to a ~25 °C increase in T_{gel} (**Fig. S9 and S10**). In contrast, an increase of pH in borax-free PVA/CNH salogels demonstrated only a slight decrease of T_{gel} (**Fig. S10**) and salogel strength as observed by the absence of crossover of *G'*(ω) and *G"*(ω) in the frequency range of 0.1-300 rad/s (**Fig. S8c** and **d**). Note that further increase of pH to 8 or 9 of PVA/borax salogels did not cause additional strengthening of the salogels (data not shown). Taken together, the data show that pH can be used is a powerful means to controlling the PVA/borax network strength and tuning its gel transition temperature.

We then aimed to compare our PVA/borax salogels with well-known PVA/borax hydrogel systems.[14, 15, 17, 20, 28, 54] For this purpose, salogels and hydrogels containing 3 wt% $PVA_{90k,98}$ and 0.16 wt% borax were prepared in CNH and water, respectively. Comparison of the storage moduli in the frequency sweep (**Fig. 5a**) and temperature sweep (**Fig. 5b**) experiments showed that the salogels were about an order of magnitude stronger than the hydrogels, while the modulus of the hydrogels was consistent with the earlier reports.[14, 17] Additionally, during frequency sweep, the hydrogels unlike the salogels showed traditional gel behavior with storage modulus (*G'*) reaching a plateau and loss modulus (*G"*) decreasing after reaching a maximum at high frequencies, whereas the borax salogels showed behavior similar to borax-free salogels discussed earlier **(Fig. S3**) and their gelation point varied by 10 °C when temperature sweeps were performed between 3 and 10 rad/s (data not shown).While the temperature sweep experiments shown in **Fig. 5b** revealed a modulus crossover for both salogels and hydrogels as an indication of temperature-triggered gel-sol transitions in both cases, the transition temperature T_{gel} occurred at a higher temperature in salogels (46 °C in comparison to 35 °C in hydrogels). The difference in T_{gel} for the salogels and hydrogels was also visualized in vial inversion experiments (**Fig. 5b)**. The higher strength of the

boronate ester salogel compared to the hydrogel can be rationalized from our earlier results in **Figs. 1** and **2** which highlight the differences in hydration of PVA in the hydrogels versus the salogels which enable additional intermolecular hydrogen bonding in PVA salogels even in the absence of borax. The strengthening of salogels by hydrogen bonds and boronate ester bonds has significant implications for shape stabilization of CNH and their application for thermal energy storage.

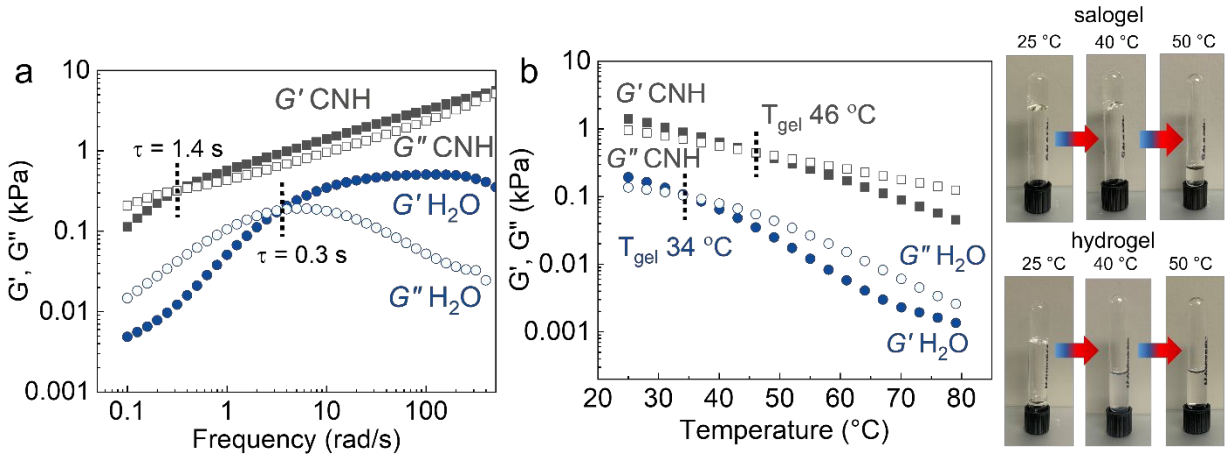

Fig. 5. Rheological behavior of PVA/borax system (3 wt% $PVA_{90k,98}$, 0.16 wt% borax) in CNH (salogels) and water (hydrogels) during (a) frequency sweep and (b) temperature sweep experiments. Images in (b) show the gel to sol transition of salogel and hydrogel upon heating above T_{gel}.

The salogels also exhibited self-healing behavior, consistent with physical gels and PVA/borax hydrogels that is supported by the transient nature of reversible crosslinking points.[55, 56] To explore the self-healing properties of PVA/borax salogels and to compare them with hydrogels, we performed step strain experiments at room temperature to probe recovery of mechanical properties of the salogels after a network rupture. These experiments first involved a strain amplitude test to determine linear viscoelastic regime for network recovery and breaking (**Fig. S11**). This was followed by step strain measurements performed between 300% and 10% strain to study the rupture and recovery of the storage and loss moduli. **Fig. 6a** and **c** show that both the salogel and hydrogel quickly recovered under 10% strain after rupturing under 300% strain. However, there were significant differences in the healing behavior of salogels and hydrogels. While the stronger salogels maintained their gel state during the rupturing step, the weaker hydrogels underwent a gel-sol transition as evidenced by the modulus crossover under 300% strain. Despite dramatically different mechanical properties and the viscoelastic behavior during rupture, both the salogels and

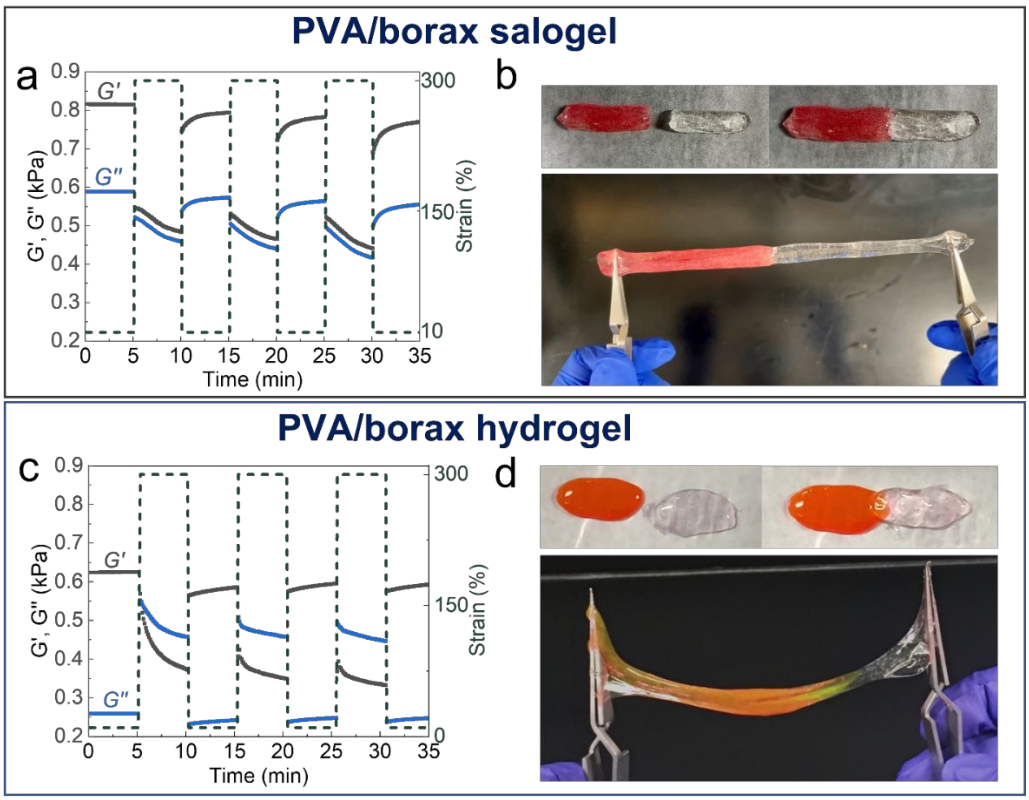

Fig. 6. Self-healing experiments for 3 wt% $PVA_{90k,98}$, 0.16 wt% borax salogels (top) and hydrogels (bottom) studied by (a, c) step-strain rheology and (b, d) visual demonstration experiments. All experiments were performed at room temperature.

hydrogels showed a similar self-healing efficiency after 5 minutes at 10% strain, as calculated from *G'* values before rupture and after recovery (**Fig. S12)**. Visual demonstration was performed from two pieces of the salogels or hydrogels (one colored with a dye and the other not) brought into contact with each other at room temperature for ten minutes for the salogels and one minute for the hydrogels to allow the self-healing to occur (**Fig. 6b, d**). The hydrogels healed faster since the weaker gel network had a shorter relaxation time allowing the boronate ester bonds to reform between the two pieces. On the other hand, the salogel pieces were more elastic and shapable as compared to the hydrogel counterparts (**Fig. 6b**), both as the original pieces and after the pieces were brought in contact and stretched. While in both cases the pieces bonded together, the material intermixing and sagging was much more severe in the case of hydrogels resulting from their more liquid-like behavior and lower mechanical strength (**Fig. 6d**).

The robustness of the salogels in shape stabilization and efficient trapping of CNH was demonstrated by heating hexagon-shaped neat CNH control and salogel samples of the

composition 3 wt% $PVA_{90k,98}$, 0.31 wt% borax to 50 °C until all the CNH melted. At ambient temperature, the CNH and salogel hexagons appeared white due to crystallization of CNH. While the polymer-free CNH hexagon could not maintain its shape due to its low viscosity and fluidity upon melting, the salogel retained its shape for 60 minutes at 50 °C (**Fig. S13**). We then proceeded to test the shape retention capability of the salogel over multiple heating/cooling cycles where the salogel was heated to 50 °C until all the CNH melted and then crystallized by cooling for 10 melting/crystallization cycles (**Fig. 7**). **Fig. 7a** shows the maintenance of the salogel shape during the 1st and 10th cycle. While slight distortion of the salogel shape caused by creep of the salogel was observed, overall good shape stabilization was achieved by a combination of physical and dynamic covalent crosslinks. It should be noted that shape stabilization was achieved with an unprecedentedly low polymer concentration (3 wt%) and low crosslinker content (0.31 wt%), not attainable with previously reported matrices.[4-8, 57, 58] The salogels containing molten CNH could be easily lifted from the substrate after the 10th melting cycle to demonstrate that there was no leakage of CNH during these cycling experiments. Moreover, the salogels were fully re-processable, and after heating above T_{gel} (70 °C) could be put back in the mold and in the freezer to recover solidified material. These experiments show that robust PVA/borax salogels can effectively trap and prevent leakage of CNH during multiple melting/freezing cycles while maximizing the content of a PCM material. The combined effects of self-healing capability, the shape stabilization, and trapping of CNH in its liquid state within the PVA/borax salogels were further demonstrated with hexagon-shaped salogels broken into two pieces, placed in contact with each other with no external pressure and heated to 50 °C for 45 minutes (**Fig. S14**). In these experiments, the two pieces healed and bonded together due to dynamic exchange of physical and dynamic covalent crosslinks. Finally, **Fig. 7b and c** illustrate the critical characteristics for the PCM applications to retain heat of fusions and PCM melting points of PCMs during repeated thermal cycling. No loss of the heat of fusion was observed, indicating no changes in the water content or the melting point of CNH in the salogel after 10 and 20 melting/crystallization cycles. These data indicate that the PVA/borax matrix did not interfere with the thermal performance of the PCM during thermal cycling.

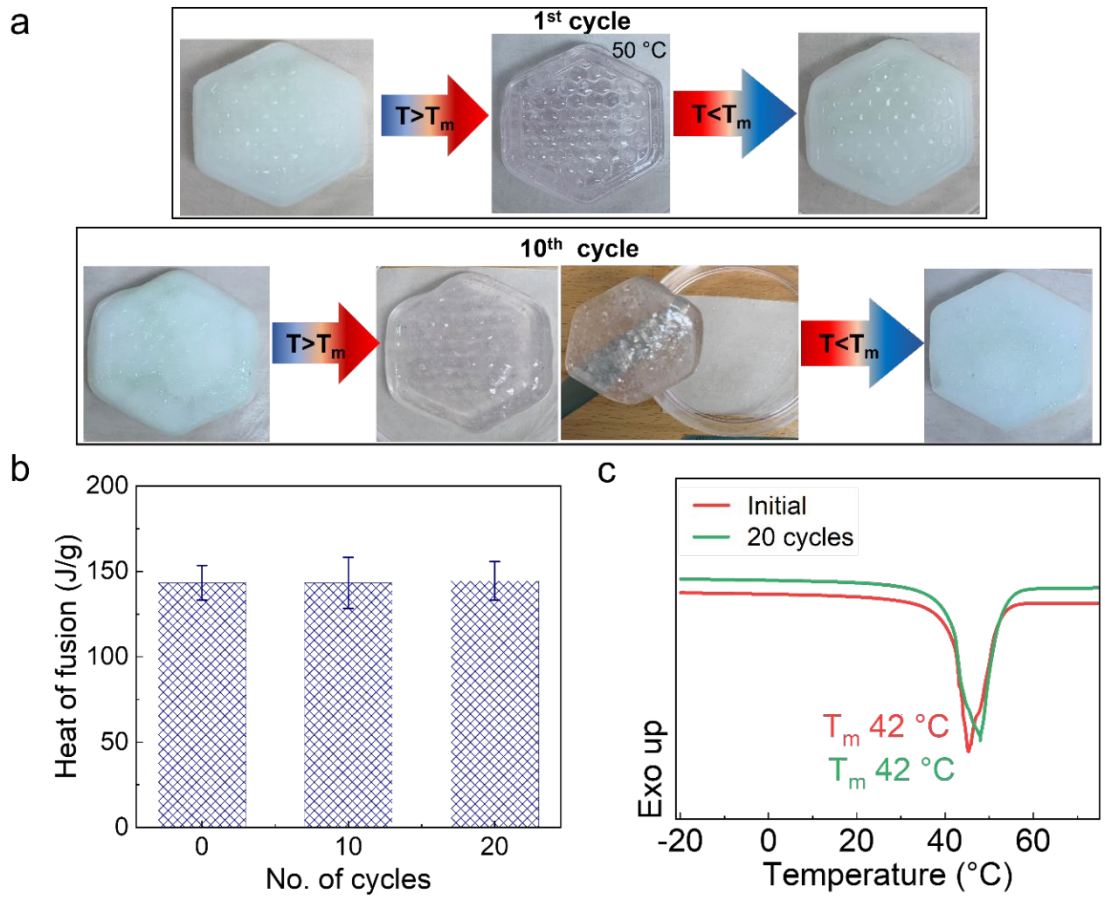

Fig 7. (a) Thermal cycling experiments showing the first and tenth cycles where the salogel was heated to 50 °C to melt the PCM and then crystallized. The pink color was due the presence of a small amount of a Rhodamine G dye added to the salogel for visualization. Preservation of (b) heat of fusion and (c) melting point during thermal cycling of 3 wt% $PVA_{90k,98}$, 0.32 wt% borax, CNH salogels.

Conclusions

In this study, strong, temperature responsive salogels with tunable T_{gel}, repeatable thermo-reversibility, and self-healing capability using dynamic covalent boronate ester bonds were reported for shape stabilization of an inorganic salt hydrate PCM. The unique environment of CNH resulted in facile gelation of PVA due to physical crosslinks, whereas the addition of borax introduced dynamic covalent crosslinks imparted strength, tunability, and thermo-reversibility of gelation. The combination of physical and dynamic covalent crosslinks resulted in salogels having superior mechanical properties and shape retention capability compared to their hydrogel

counterparts. The suitability of PVA/borax salogels for thermal energy storage applications was demonstrated by shape stabilization experiments in which the salogels showed capability of trapping a very high loading level of the PCM (>96 wt% CNH) in the salogel matrix. The thermal properties of CNH were preserved in the salogel with more than 95% of the heat of fusion of neat CNH being retained and maintained over multiple melting/crystallization cycles, illustrating their promise for thermal energy storage applications.

Author contributions

K. K. R. contributed with methodology development, project administration, visualization, investigation, formal analysis, and validation, writing of original draft, reviewing, and editing of manuscript. X. Z. contributed with investigation, formal analysis and validation, visualization, writing original draft of the manuscript. S.A.S. contributed with conceptualization, funding acquisition, providing resources, supervision, project administration, visualization, and led reviewing and editing of the manuscript.

Conflicts of interest

The authors declare no conflicts of interest.

Acknowledgements

This material is based upon work supported by the U.S. Department of Energy's Office of Energy Efficiency and Renewable Energy (EERE) under the Buildings and Technologies Award Number DE-EE0009155, as well as work supported by the National Science Foundation under Grant No. 1847956**.** We also acknowledge the use of Soft Matter Facility for testing.

References

1. Alva, G.; Lin, Y.; Fang, G., An overview of thermal energy storage systems. *Energy* **2018,** *144*, 341-378.
2. Telkes, M., Thermal energy storage in salt hydrates. *Solar Energy Materials* **1980,** *2* (4), 381-393.
3. Rajagopalan, K. K.; Karimineghlani, P.; Zhu, X.; Shamberger, P. J.; Sukhishvili, S. A., Polymers in molten inorganic salt hydrate phase change materials: solubility and gelation. *Journal of Materials Chemistry A* **2021,** *9*, 25892-25913.
4. Yin, C.; Lan, J.; Wang, X.; Zhang, Y.; Ran, R.; Shi, L.-Y., Shape-Stable Hydrated Salts/Polyacrylamide Phase-Change Organohydrogels for Smart Temperature Management. *ACS Applied Materials & Interfaces* **2021,** *13* (18), 21810-21821.
5. Liu, Y.; Yu, K.; Xie, M.; Lu, S.; Yang, Y.; Wang, H.; Jia, H., Hydrate salt/self-curing acrylic resin form-stable phase change materials with enhanced surface stability and thermal properties via the incorporation of graphene oxide. *International Journal of Energy Research* **2020,** *44* (7), 5791-5805.
6. Yu, K.; Liu, Y.; Sun, F.; Jia, M.; Yang, Y., Graphene-Modified Hydrate Salt/UV-Curable Resin Form-Stable Phase Change Materials: Continuously Adjustable Phase Change Temperature and Ultrafast Solar-to-Thermal Conversion. *Energy & Fuels* **2019,** *33* (8), 7634-7644.
7. Liu, Y.; Yu, K.; Gao, X.; Ren, M.; Jia, M.; Yang, Y., Enhanced thermal properties of hydrate salt/poly (acrylate sodium) copolymer hydrogel as form-stable phase change material via incorporation of hydroxyl carbon nanotubes. *Solar Energy Materials and Solar Cells* **2020,** *208*, 110387.
8. Wang, T.; Wu, N.; Li, H.; Lu, Q.-L.; Jiang, Y., Preparation and properties of a form-stable phase-change hydrogel for thermal energy storage. *Journal of Applied Polymer Science* **2016,** *133* (34).
9. Karimineghlani, P.; Emmons, E.; Green, M. J.; Shamberger, P.; Sukhishvili, S. A., A temperature-responsive poly (vinyl alcohol) gel for controlling fluidity of an inorganic phase change material. *Journal of Materials Chemistry A* **2017,** *5* (24), 12474-12482.
10. Karimineghlani, P.; Palanisamy, A.; Sukhishvili, S. A., Self-Healing Phase Change Salogels with Tunable Gelation Temperature. *ACS Applied Materials & Interfaces* **2018,** *10* (17), 14786-14795.
11. Karimineghlani, P.; Zheng, J.; Hu, Y.-Y.; Sukhishvili, S., Solvation and diffusion of poly (vinyl alcohol) chains in a hydrated inorganic ionic liquid. *Physical Chemistry Chemical Physics* **2020,** *22* (31), 17705-17712.
12. Fischer, S.; Leipner, H.; Thümmler, K.; Brendler, E.; Peters, J., Inorganic molten salts as solvents for cellulose. *Cellulose* **2003,** *10* (3), 227-236.
13. Karimineghlani, P.; Sukhishvili, S. A., Activation Energy for Dissociation of Hydrogen-Bonding Crosslinkers in Phase-Change Salogels: Dynamic Light Scattering versus Rheological Studies. *Macromolecular Chemistry and Physics* **2019,** *220* (22), 1900329.
14. Cho, S.; Hwang, S. Y.; Oh, D. X.; Park, J., Recent progress in self-healing polymers and hydrogels based on reversible dynamic B–O bonds: boronic/boronate esters, borax, and benzoxaborole. *Journal of Materials Chemistry A* **2021,** *9* (26), 14630-14655.
15. Dixit, A.; Bag, D. S.; Kalra, S., Synthesis of strong and stretchable double network (DN) hydrogels of PVA-borax and P (AM-co-HEMA) and study of their swelling kinetics and mechanical properties. *Polymer* **2017,** *119*, 263-273.

16. Gao, L.; Guo, G.; Liu, M.; Tang, Z.; Xie, L.; Huo, Y., Multi-responsive, bidirectional, and large deformation bending actuators based on borax cross-linked polyvinyl alcohol derivative hydrogel. *RSC Advances* **2017,** *7* (63), 40005-40014.
17. Han, J.; Lei, T.; Wu, Q., High-water-content mouldable polyvinyl alcohol-borax hydrogels reinforced by well-dispersed cellulose nanoparticles: Dynamic rheological properties and hydrogel formation mechanism. *Carbohydrate Polymers* **2014,** *102*, 306-316.
18. Seidi, F.; Jin, Y.; Han, J.; Saeb, M. R.; Akbari, A.; Hosseini, S. H.; Shabanian, M.; Xiao, H., Self-healing Polyol/Borax Hydrogels: Fabrications, Properties and Applications. *The Chemical Record* **2020,** *20* (10), 1142-1162.
19. Murphy, D. J.; Sankalia, M. G.; Loughlin, R. G.; Donnelly, R. F.; Jenkins, M. G.; McArron, P. A., Physical characterisation and component release of poly(vinyl alcohol)–tetrahydroxyborate hydrogels and their applicability as potential topical drug delivery systems. *International Journal of Pharmaceutics* **2012,** *423* (2), 326-334.
20. Wang, C.; Shen, Z.; Hu, P.; Wang, T.; Zhang, X.; Liang, L.; Bai, J.; Qiu, L.; Lai, X.; Yang, X.; Zhang, K., Facile fabrication and characterization of high-performance Borax-PVA hydrogel. *Journal of Sol-Gel Science and Technology* **2022,** *101* (1), 103-113.
21. Redy Keisar, O.; Nahum, V.; Yehezkel, L.; Marcovitch, I.; Columbus, I.; Fridkin, G.; Chen, R., Active and Strippable PVA/Borax/NaBO3 Hydrogel for Effective Containment and Decontamination of Chemical Warfare Agents. *ACS Omega* **2021,** *6* (8), 5359-5367.
22. Liu, C.; Lei, F.; Li, P.; Wang, K.; Jiang, J., A review on preparations, properties, and applications of cis-ortho-hydroxyl polysaccharides hydrogels crosslinked with borax. *International Journal of Biological Macromolecules* **2021,** *182*, 1179-1191.
23. He, L.; Szopinski, D.; Wu, Y.; Luinstra, G. A.; Theato, P., Toward Self-Healing Hydrogels Using One-Pot Thiol–Ene Click and Borax-Diol Chemistry. *ACS Macro Letters* **2015,** *4* (7), 673-678.
24. Lu, B.; Lin, F.; Jiang, X.; Cheng, J.; Lu, Q.; Song, J.; Chen, C.; Huang, B., One-pot assembly of microfibrillated cellulose reinforced PVA–borax hydrogels with self-healing and pH-responsive properties. *ACS Sustainable Chemistry & Engineering* **2017,** *5* (1), 948-956.
25. Rezvan, G.; Pircheraghi, G.; Bagheri, R., Curcumin incorporated PVA-borax dual delivery hydrogels as potential wound dressing materials—Correlation between viscoelastic properties and curcumin release rate. *Journal of Applied Polymer Science* **2018,** *135* (45), 46734.
26. Carretti, E.; Grassi, S.; Cossalter, M.; Natali, I.; Caminati, G.; Weiss, R. G.; Baglioni, P.; Dei, L., Poly(vinyl alcohol)−Borate Hydro/Cosolvent Gels: Viscoelastic Properties, Solubilizing Power, and Application to Art Conservation. *Langmuir* **2009,** *25* (15), 8656-8662.
27. Ding, Q.; Xu, X.; Yue, Y.; Mei, C.; Huang, C.; Jiang, S.; Wu, Q.; Han, J., Nanocellulose-Mediated Electroconductive Self-Healing Hydrogels with High Strength, Plasticity, Viscoelasticity, Stretchability, and Biocompatibility toward Multifunctional Applications. *ACS Applied Materials & Interfaces* **2018,** *10* (33), 27987-28002.
28. Lin, H.-L.; Liu, Y.-F.; Yu, T. L.; Liu, W.-H.; Rwei, S.-P., Light scattering and viscoelasticity study of poly (vinyl alcohol)–borax aqueous solutions and gels. *Polymer* **2005,** *46* (15), 5541-5549.
29. Pezron, E.; Leibler, L.; Ricard, A.; Audebert, R., Reversible gel formation induced by ion complexation. 2. Phase diagrams. *Macromolecules* **1988,** *21* (4), 1126-1131.
30. Koike, A.; Nemoto, N.; Inoue, T.; Osaki, K., Dynamic Light Scattering and Dynamic Viscoelasticity of Poly(vinyl alcohol) in Aqueous Borax Solutions. 2. Polymer Concentration and Molecular Weight Effects. *Macromolecules* **1995,** *28* (7), 2339-2344.

31. Moynihan, C. T., A low temperature fused salt experiment: The conductivity, viscosity, and density of molten calcium nitrate tetrahydrate. *Journal of Chemical Education* **1967,** *44* (9), 531.
32. Moynihan, C. T., The Temperature Dependence of Transport Properties of Ionic Liquids. The Conductance and Viscosity of Calcium Nitrate Tetrahydrate and Sodium Thiosulfate Pentahydrate. *The Journal of Physical Chemistry* **1966,** *70* (11), 3399-3403.
33. Xu, M.; Larentzos, J. P.; Roshdy, M.; Criscenti, L. J.; Allen, H. C., Aqueous divalent metal–nitrate interactions: hydration versus ion pairing. *Physical Chemistry Chemical Physics* **2008,** *10* (32), 4793-4801.
34. Sharma, A.; Tyagi, V. V.; Chen, C.; Buddhi, D., Review on thermal energy storage with phase change materials and applications. *Renewable and Sustainable Energy Reviews* **2009,** *13* (2), 318-345.
35. Sun, Q., The Raman OH stretching bands of liquid water. *Vibrational Spectroscopy* **2009,** *51* (2), 213-217.
36. Sun, Q.; Guo, Y., Vibrational sum frequency generation spectroscopy of the air/water interface. *Journal of Molecular Liquids* **2016,** *213*, 28-32.
37. Ludwig, R., Water: From clusters to the bulk. *Angewandte Chemie International Edition* **2001,** *40* (10), 1808-1827.
38. Tsai, C.; Jordan, K., Theoretical study of small water clusters: low-energy fused cubic structures for $(H_2O)_n$, n = 8, 12, 16, and 20. *The Journal of Physical Chemistry* **1993,** *97* (20), 5208-5210.
39. Su, W.; Darkwa, J.; Kokogiannakis, G., Review of solid–liquid phase change materials and their encapsulation technologies. *Renewable and Sustainable Energy Reviews* **2015,** *48*, 373-391.
40. Peppas, N. A.; Stauffer, S. R., Reinforced uncrosslinked poly (vinyl alcohol) gels produced by cyclic freezing-thawing processes: a short review. *Journal of Controlled Release* **1991,** *16* (3), 305-310.
41. Holloway, J. L.; Lowman, A. M.; Palmese, G. R., The role of crystallization and phase separation in the formation of physically cross-linked PVA hydrogels. *Soft Matter* **2013,** *9* (3), 826-833.
42. Di Biase, M.; de Leonardis, P.; Castelletto, V.; Hamley, I. W.; Derby, B.; Tirelli, N., Photopolymerization of Pluronic F127 diacrylate: a colloid-templated polymerization. *Soft Matter* **2011,** *7* (10), 4928-4937.
43. Winter, H. H.; Chambon, F., Analysis of linear viscoelasticity of a crosslinking polymer at the gel point. *Journal of Rheology* **1986,** *30* (2), 367-382.
44. Winter, H. H., Can the gel point of a cross-linking polymer be detected by the G′–G ″ crossover? *Polymer Engineering & Science* **1987,** *27* (22), 1698-1702.
45. Liu, M.; Lu, X.; Gao, L.; Wang, S.; Huo, Y.; Chen, Z. N., Polyvinyl Alcohol-Based Thermogel with Tunable Gelation and Self-Healing Property. *Macromolecular Chemistry and Physics* **2018,** *219* (14), 1800162.
46. Zhang, Z. X.; Liu, K. L.; Li, J., A Thermoresponsive Hydrogel Formed from a Star–Star Supramolecular Architecture. *Angewandte Chemie International Edition* **2013,** *52* (24), 6180-6184.
47. Schultz, R. K.; Myers, R. R., The Chemorheology of Poly(vinyl alcohol)-Borate Gels. *Macromolecules* **1969,** *2* (3), 281-285.

48. Nijenhuis, K., Poly(vinyl alcohol). In *Thermoreversible Networks: Viscoelastic Properties and Structure of Gels*, Springer Berlin Heidelberg: Berlin, Heidelberg, 1997; pp 37-66.
49. Wu, D.; Shi, Y.; Lv, K.; Wei, B.; Zhu, Y.; Yin, H.; Feng, Y., Tunable Viscoelastic Properties of Sodium Polyacrylate Solution via CO2-Responsive Switchable Water. *Molecules* **2021,** *26* (13), 3840.
50. Shen, D.; Wan, C.; Gao, S., Molecular weight effects on gelation and rheological properties of konjac glucomannan–xanthan mixtures. *Journal of Polymer Science Part B: Polymer Physics* **2010,** *48* (3), 313-321.
51. Wang, Q.; Li, L., Effects of molecular weight on thermoreversible gelation and gel elasticity of methylcellulose in aqueous solution. *Carbohydrate Polymers* **2005,** *62* (3), 232-238.
52. Muppalaneni, S.; Omidian, H., Polyvinyl Alcohol in Medicine and Pharmacy: A Perspective. *Journal of Developing Drugs* **2013,** *2* (3), 1-5.
53. Koga, K.; Takada, A.; Nemoto, N., Dynamic Light Scattering and Dynamic Viscoelasticity of Poly (vinyl alcohol) in Aqueous Borax Solutions. 5. Temperature Effects. *Macromolecules* **1999,** *32* (26), 8872-8879.
54. Huang, M.; Hou, Y.; Li, Y.; Wang, D.; Zhang, L., High performances of dual network PVA hydrogel modified by PVP using borax as the structure-forming accelerator. *Designed Monomers and Polymers* **2017,** *20* (1), 505-513.
55. Yang, Y.; Urban, M. W., Self-healing polymeric materials. *Chemical Society Reviews* **2013,** *42* (17), 7446-7467.
56. Zhao, Z.; Liu, Y.; Zhang, K.; Zhuo, S.; Fang, R.; Zhang, J.; Jiang, L.; Liu, M., Biphasic Synergistic Gel Materials with Switchable Mechanics and Self-Healing Capacity. *Angewandte Chemie* **2017,** *129* (43), 13649-13654.
57. Bao, X.; Yang, H.; Xu, X.; Xu, T.; Cui, H.; Tang, W.; Sang, G.; Fung, W., Development of a stable inorganic phase change material for thermal energy storage in buildings. *Solar Energy Materials and Solar Cells* **2020,** *208*, 110420.
58. Xiao, Q.; Fan, J.; Li, L.; Xu, T.; Yuan, W., Solar thermal energy storage based on sodium acetate trihydrate phase change hydrogels with excellent light-to-thermal conversion performance. *Energy* **2018,** *165*, 1240-1247.